NeuroImage 52 (2010) 1135–1147

Contents lists available at ScienceDirect

NeuroImage

journal homepage: www.elsevier.com/locate/ynimg

# A dynamic model of neurovascular coupling: Implications for blood vessel dilation and constriction

Ying Zheng [a,*], Yi Pan [a], Sam Harris [a], Steve Billings [b], Daniel Coca [b], Jason Berwick [a], Myles Jones [a], Aneurin Kennerley [a], David Johnston [a], Chris Martin [c], Ian M. Devonshire [d], John Mayhew [a]

[a] Centre for Signal Processing in Neuro-imaging and Systems Neuroscience, Department of Psychology, University of Sheffield, Northumberland Road, Sheffield S10 2TP, UK
[b] Centre for Signal Processing in Neuro-imaging and Systems Neuroscience, Department of Automatic Control and Systems Engineering, University of Sheffield, S1 3JD, UK
[c] Radiobiology Research Institute, University of Oxford, Churchill Hospital, Headington, Oxford OX3 7LJ, UK
[d] Department of Pharmacology, University of Oxford, Mansfield Road, Oxford, OX1 3QT, UK

ARTICLE INFO

*Article history:*
Received 1 August 2009
Revised 27 January 2010
Accepted 28 January 2010
Available online 4 February 2010

ABSTRACT

Neurovascular coupling in response to stimulation of the rat barrel cortex was investigated using concurrent multichannel electrophysiology and laser Doppler flowmetry. The data were used to build a linear dynamic model relating neural activity to blood flow. Local field potential time series were subject to current source density analysis, and the time series of a layer IV sink of the barrel cortex was used as the input to the model. The model output was the time series of the changes in regional cerebral blood flow (CBF). We show that this model can provide excellent fit of the CBF responses for stimulus durations of up to 16 s. The structure of the model consisted of two coupled components representing vascular dilation and constriction. The complex temporal characteristics of the CBF time series were reproduced by the relatively simple balance of these two components. We show that the impulse response obtained under the 16-s duration stimulation condition generalised to provide a good prediction to the data from the shorter duration stimulation conditions. Furthermore, by optimising three out of the total of nine model parameters, the variability in the data can be well accounted for over a wide range of stimulus conditions. By establishing linearity, classic system analysis methods can be used to generate and explore a range of equivalent model structures (e.g., feed-forward or feedback) to guide the experimental investigation of the control of vascular dilation and constriction following stimulation.



## Introduction

When neurons are activated, a change in regional blood flow typically occurs. The relationship between changes in neural activity and the ensuing changes in the regional cerebral blood flow, known as neurovascular coupling, has been an area of intensive research. Understanding this relationship is crucial to how we interpret brain signals measured via non-invasive neuroimaging techniques such as functional magnetic resonance imaging (fMRI), as these techniques measure changes in the regional cerebral haemodynamic responses (e.g., blood flow, blood volume, and blood oxygenation state) to make inferences about the underlying neural activity.

Reviews on neurovascular coupling studies at the cellular level can be found in Hamel (2006) and Iadecola and Nedergaard (2007). *In vitro* and *in vivo* studies have shown that an increase in neural activity releases vasoactive agents. With astrocytes acting as mediators, some of these agents induce the adjacent blood vessels to dilate or constrict, or both (Filosa and Blanco, 2007; Metea and Newman, 2006; Mulligan and MacVicar, 2004; Stefanovic et al., 2007; Zonta et al., 2003). Furthermore, the oxygen concentration in the brain tissue within the region of increased neural activity has also been implicated, in an *in vitro* study, as a mediating factor in determining whether the blood vessels dilate or constrict (Gordon et al., 2008).

Utilising experimental findings at the cellular level, several models of neurovascular coupling have been proposed linking changes in neural activity to changes in cerebral blood flow or volume via various cellular mechanisms (Aubert and Costalat, 2002; Bennett et al., 2008; Riera et al., 2007, 2006). These models tend to include a large number of physiological variables that are involved in the underlying process of neurovascular coupling.

At a different level, many studies of neurovascular coupling have used the concurrent recording of neural activity while monitoring the haemodynamic responses to stimulation. These studies frequently use steady-state analysis as well as dynamic modelling to relate the changes in neural activity to the evoked changes in the haemodynamic responses (Ances et al., 2000; Hewson-Stoate et al., 2005; Jones et al., 2004; Lauritzen, 2001; Li and Freeman, 2007; Martindale et al., 2005; Mathiesen et al., 1998; Nikos, 2002; Rasmussen et al., 2009; Sheth et al., 2004; Thompson et al., 2004; Ureshi et al., 2004). The general consensus from these investigations seems to be that, from the signal processing point of view, neurovascular coupling may be linear within a narrow range of stimulus parameters, for example, for brief stimulation durations (less than 2 s) and at reasonable

* Corresponding author. Fax: +44 114 276 6515.
*E-mail address:* ying.zheng@shef.ac.uk (Y. Zheng).

1053-8119/$ – see front matter © 2010 Elsevier Inc. All rights reserved.
doi:10.1016/j.neuroimage.2010.01.102

stimulation intensities, but becomes nonlinear if the stimulation parameters are outside this narrow range.

Beside these data-driven modelling studies, some very simple dynamic models of neurovascular coupling have been proposed (Buxton et al., 2004; Friston et al., 2000) and used in modelling the relationship between changes in neural activity and the blood oxygen level-dependent (BOLD) signals obtained in fMRI studies (Blockley et al., 2009; Riera et al., 2004; Sotero and Trujillo-Barreto, 2007, 2008; Zheng et al., 2002). It is important to recognise that these simplistic models of neurovascular coupling are not directly validated by experimental data.

In this article, we identify a formal model of the relationship between changes in neural activity and the cerebral blood flow (CBF) time series using experimental data and demonstrate that this relationship can be modelled by a linear dynamic model over stimulus durations of up to 16 s. The model, inspired by the varied and complex temporal characteristics of the CBF time series, is time-invariant, or autonomous. This means that the parameters of the model are not functions of time and that the dynamic relationship between the input (neural activity) and the output (CBF) of the model does not change over the entire time course of the response, including both the stimulus onset period and the haemodynamic refractory period (Huettel and McCarthy, 2001). An important feature of the model is that its structure incorporates a dilation component and a constriction component. We demonstrate, using simulation, that by changing the relative contributions of these two components, the model is able to generate the wide range of complex temporal characteristics (shapes) of the CBF responses, which have been described in the literature. The model is tested and validated against data from experiments measuring the electrophysiological and CBF responses to stimulation of the rat whisker pad. The importance of the establishment of the linearity of neurovascular coupling for future research is discussed.

## Materials and methods

For detailed experimental procedures, the reader is directed to Jones et al (2004) and Hewson-Stoate et al. (2005) for reference. They are briefly reviewed below.

### *Animal preparation*

The animals used were Hooded Lister rats weighing between 200 and 300 g, anaesthetised with urethane (1.25 g/kg intraperitoneal injection), and atropine (0.4 ml/kg subcutaneous injection, 600 μg/ml) was used to reduce mucous secretions. The animals were placed in a stereotaxic holder (Kopf Instruments), and the skull overlying the whisker barrel cortex was thinned to translucency with a dental drill under constant cooling with saline. Rectal temperature was maintained at ~37 °C with a thermostatic heating pad. ECG electrodes were attached to monitor heart rate. A tracheotomy was performed to enable artificial ventilation (20% $O_2$, 80% $N_2$, 1–1.3 Hz). The left femoral vein and artery were cannulated to allow drug infusion of Phenylephrine (0.13–0.26 mg/h) and measurement of mean arterial blood pressure, respectively. The rate of Phenylephrine infusion was varied to keep MABP within the normal physiological range (100–110 mm Hg). Physiological parameters were continuously monitored and maintained within normal ranges (mean ± SE: $PO_2$: 93.1 ± 0.24 mm Hg, $PCO_2$: 28.7 ± 0.27 mm Hg, $S_{O2}$: 96.9 ± 0.03%, pH: 7.34 ± 0.002).

### *Electrophysiology and laser Doppler flowmetry (LDF)*

The whisker barrel cortex region was located using optical imaging of intrinsic signals (590-nm illumination) and electrical stimulation of the contralateral whisker pad. Subsequent optical imaging maps were aligned to images of the cortical surface and used to guide placement of electrode and LDF probes. Electrophysiological recordings were made using an electrode probe, which consisted of a linear array of 16 electrode sites (100 μm spacing, area of each site: 177 $\mu m^2$, impedance: 1.5–2.7 MΩ, probing width: 33 μm at tip, 123 μm at uppermost electrode; NeuroNexus Technologies, University of Michigan) coupled to a data acquisition device (TDT, Florida) with a custom-written Matlab interface. A small hole in the skull and dura in the centre of the 'active' cortical region were made, and the electrode was inserted normal to cortical surface by hydraulic micromanipulator control (Narishige—1 μm accuracy in the '*z*-axis', i.e., that corresponding to cortical depth) under micromanipulator control such that the lowermost electrode of the array was placed at a depth of ~1500 μm. The evoked field potential recordings were sampled at 6103.5 Hz with 16-bit resolution. The LDF probe (PeriFlux 5010, Perimed, Stockholm, 780 nm illumination, 0.25 mm separation) was placed under visual guidance (Leica MZ 7.5 stereomicroscope—×60 magnification) such that it overlays the cortical surface (<1 mm) and that the maximum distance from the LDF probe to the uppermost channel of the multi-channel electrode was approximately 100 μm in the *x*–*y* plane. The LDF spectrometer included a low-pass filter with a 0.2-s time constant and 12-kHz bandwidth (Nilsson, 1984) to reduce errors caused by measurement noise. The LDF has a sampling rate of 30 Hz and was used to measure changes in CBF concurrently with electrophysiological recordings. The CBF changes were normalised with respect to the baseline CBF collected for a period of 8 s prior to the onset of each trial.

Multi-laminar measures of evoked field potentials enabled the use of current source density (CSD) analysis, which resolves the spatial ambiguities inherent in evoked field potential recordings into a laminar distribution of current sinks and sources. Electrical whisker pad stimuli result in a large sink-source dipole towards the surface of the cortex. As sinks reflect active excitatory postsynaptic potentials (EPSPs) rather than passive (e.g., sources) neural mechanisms, we have typically compared the evoked sinks rather than sources with the accompanying haemodynamics (e.g., see Martindale et al., 2003, and Jones et al., 2004). This 'primary' current sink has previously been found to co-localise extremely well with layer IV (about 450 μm below the surface of the cortex) as visualised by cytochrome oxidase histology (Jones et al., 2004). An autoradiography study (Gerrits et al., 2000) has shown that maximal CBF (both at rest and during stimulation) is also observed in layer IV. Furthermore, if the matrix of the CSD analysis is subject to principal components analysis, this aspect of the response accounts for >80% of the variance of the matrix (Martindale et al., 2003). Thus CSD data and LDF data (which is a spatial average over depths) have their major signal sources co-localised in layer IV. For this reason, time series of the layer IV CSD sink were used as the basis of the 'incoming' neural activity and intracortical processing (Martindale et al., 2003), from which temporal profiles of the CSD analysis were extracted. Comparing this aspect of the neural response with the accompanying haemodynamics is thus justified from both a signal processing and neurophysiological perspective.

As the width of a CSD response to an individual of a stimulus train is around 10 ms, the CSD responses were down-sampled to 90 Hz to save 'computational' time, and each CSD 'spike' was represented by a single pulse in the down-sampled sequence whose amplitude was modulated by the corresponding temporal profile (sign inverted) of the CSD response. Per animal, the CSD profiles were normalised so that the mean first pulse over all trials was unity. Hence the neural signals used throughout this article were the modified CSD pulse trains with a pulse width of 1/90 s (or 11 ms).

### *Experimental paradigms*

Electrical stimulation of the whisker pad was delivered in 5 Hz trains with each pulse having an intensity of 1.2 mA and an individual pulse width of 0.3 ms. The duration of the stimulus train was varied.

Experimental paradigms were specifically designed to have a conditioning block of stimulation followed closely in time by a probing block of stimulation per trial instead of the traditional single block of stimulus. The objectives of such design are two-fold: one is to investigate neural adaptation and recovery characteristics (work in progress), the other is to ensure that any mathematical models of neurovascular coupling we identify are capable of fitting the CBF response with respect to not only the conditioning block but also the probing block of stimulation whose onset occurs well within the return-to-baseline period of the CBF response to the conditioning block. Hence the two-block design improved on previous work (Martindale et al., 2005; Rosengarten et al., 2003) by enforcing the requirement that the mathematical model deals with the CBF response both during stimulation and during the return-to-baseline period.

Two experimental paradigms were used here. The first one was used to identify a dynamic model linking neural activity to change in the regional CBF. The second paradigm was used for model validation purpose.

*Paradigm 1*

Two blocks of stimuli were used for each trial ((Fig. 1(a))). The first conditioning block has variable duration (2, 8, or 16 s), followed by the second probing block of 1-s fixed duration. The time interval between the two blocks of stimulation also varies with seven intervals (0.6, 1, 2, 3, 4, 6, or 8 s). We will refer to this interval as the inter-block-stimulus interval (IBSI). Thus there are 21 types of stimulus presentation trials. Each trial lasted 60 s, and each experimental run consists of the 21 trials arranged in a random order. Each run was repeated 10 times per animal, resulting in each trial being repeated 10 times over the entire period of the experiment. Data were then animal averaged ($n=11$).

*Paradigm 2*

Again two blocks of stimuli were used for each trial (Fig. 1(b)). The conditioning block has variable duration (2, 4, 8, or 16 s), followed by the probing block of 2-s fixed duration. The IBSI was also fixed at 2 s. Each stimulus condition lasted 60 s, arranged in random order, and repeated three times per experimental run. Ten runs were performed per animal, resulting in each trial being repeated 30 times per experiment. Data were averaged over 5 animals.

*A simulation of haemodynamic responses*

The temporal characteristics of haemodynamic responses (mainly blood flow and volume) to long duration stimulation are often characterised by an initial overshoot followed by a 'plateau' or 'ramp' during the onset of stimulation. However, the initial overshoot is not always observed (Kida et al., 2007; Mandeville et al., 1999; Vazquez et al., 2008). Following cessation of stimulation, the haemodynamic response typically decreases rapidly and is then followed by a much slower return-to-baseline time course (Berwick et al., 2005; Herman et al., 2008; Jones et al., 2002; Kennerley et al., 2005).

An intriguing characteristic of the haemodynamic response often observed but rarely discussed in the literature is that during the return-to-baseline phase, the CBF can exhibit a marked temporal increase immediately following the rapid decrease phase before it returns to baseline slowly. This temporal characteristic can be readily observed in our CBF data shown in Fig. 2. For trials with 16-s conditioning block (Fig. 2(c)), it can be seen that CBF starts to increase slightly 4 s after stimulus cessation before it decreases to baseline. Fig. 2(d) displays a single CBF time series, which demonstrates this temporal increase more clearly. The same characteristic is present for the 8-s conditions (Fig. 2(b)), and even for the 2-s conditions (Fig. 2(a)), there is evidence of slight increase in the haemodynamic responses, although this is very much masked by the noise present at baseline.

The timing of this increase in CBF during the return to baseline phase seems independent of the duration of stimulation and the IBSIs, indicating that it is not associated with vasomotion (Mayhew et al., 1996) or the subjects' anticipation of the probing stimulus. This haemodynamic characteristic can also be observed in other published

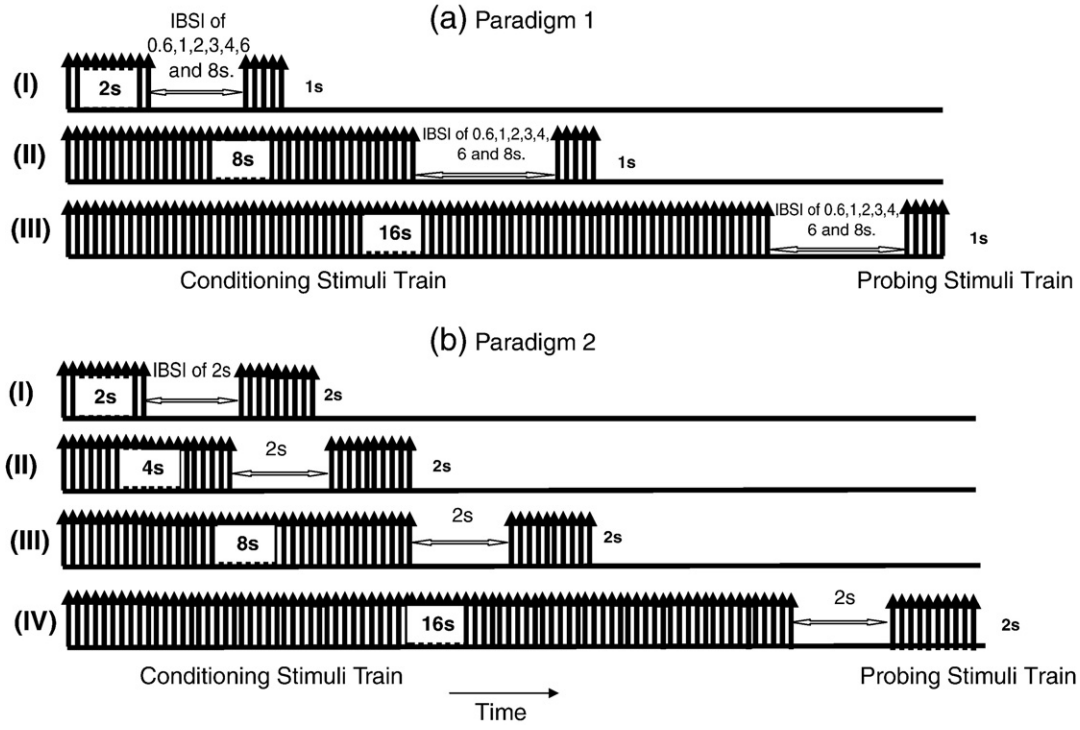


**Fig. 1.** Experimental paradigms. For each paradigm, two blocks of stimuli were used each with stimulation frequency of 5 Hz. (a) Stimulation sequences for paradigm 1. The conditioning block has a variable duration of 2, 8, and 16 s, respectively. The probing block has a fixed duration of 1 s. The IBSI varies from 0.6 to 1, 2, 3, 4, 6, and 8 s. (b) Stimulation sequences for paradigm 2. The conditioning block has a variable duration of 2, 4, 8, and 16 s, respectively. The probing block has a fixed duration of 2 s. The IBSI is also fixed at 2 s.

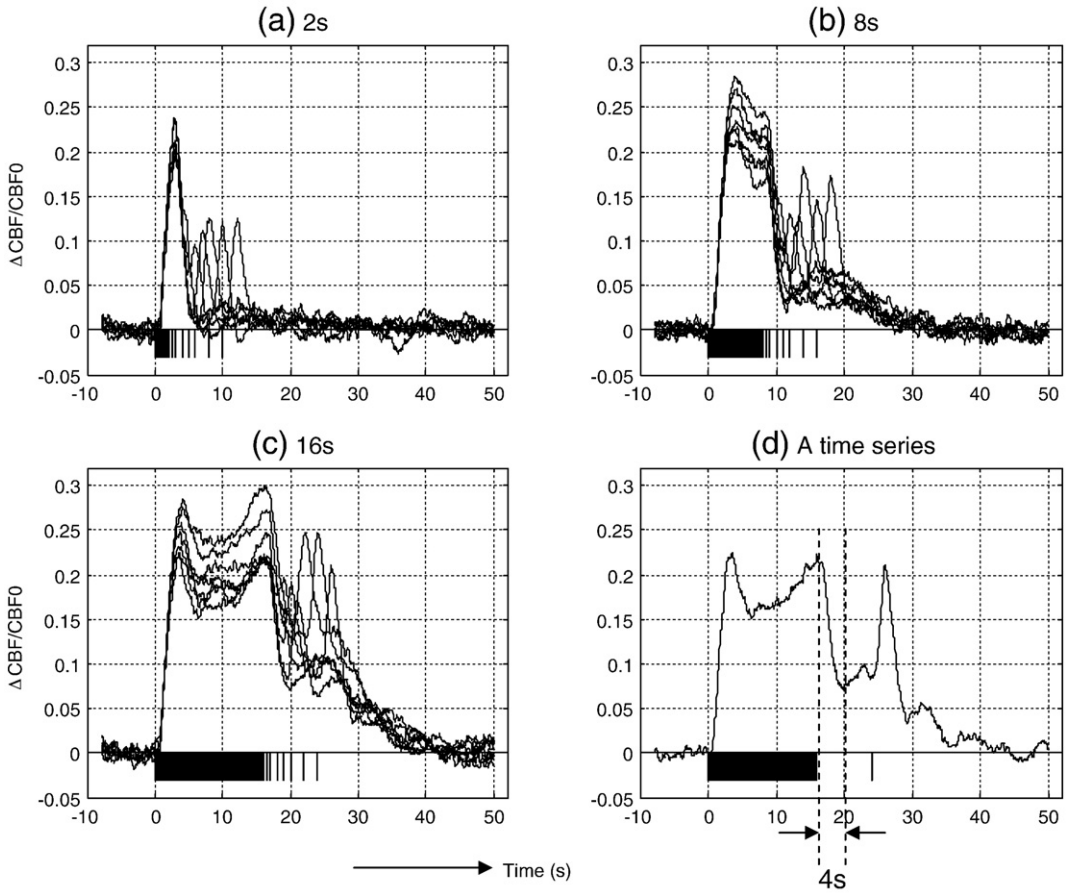


**Fig. 2.** Time series of cortical normalised CBF changes following presentation of electrical whisker pad stimuli. The black bar on the time axis indicates the stimulus duration of the conditioning block. The vertical black lines along the time axis indicate the onset time of the probing stimulus corresponding to each IBSI. (a) Two-second duration conditions; (b) 8-s duration conditions; and (c) 16-s duration conditions. Each plot has seven animal-and-trial-averaged time series superimposed, corresponding to the seven different IBSIs: 0.6, 1, 2, 3, 4, 6 and 8 s. (d) A single time series of the normalised CBF with the conditioning block duration of 16 s and the IBSI of 8 s. Approximately 4 s after the cessation of the conditioning block stimuli, CBF starts to increase well before the onset of the probing block of stimulation.

work (Berwick et al., 2005; Herman et al., 2008; Kennerley et al., 2005; Kida et al., 2007). In awake animals, this feature seems to be more prominent (Martin et al., 2009).

The crucial question is, why does the haemodynamic response not return to baseline monotonically while the neural response (in terms of CSD) has ceased?

The complex temporal characteristics of the haemodynamic responses suggest that there might be two components in the vascular response to the evoked neural activity, one has the dilating effect and the other constricting effect, and the two components are not exactly in phase with each other. resulting in the observed temporal characteristics in the vascular response. To investigate this hypothesis, a simulation was conducted in which two time series of typical 'bump' functions $y_1(t)$ and $y_2(t)$ were generated using two linear dynamic systems (see Appendix A). They were then subtracted from each other in different ratios. Time series representative of the temporal characteristics of the resultant signal $y_1(t)-y_2(t)$, are shown in the Results section where it can be seen that the spectrum of the shapes of the haemodynamic responses is easily mimicked.

*The dynamic model of dilation and constriction*

Based on the results of the simulation and the insights from the neurovascular coupling research conducted at the cellular level (Filosa and Blanco, 2007; Metea and Newman, 2006), we hypothesise that the dynamic characteristics of the CBF time series are the result of blood vessels dilating and constricting simultaneously with different time constants and magnitudes. A linear dynamic model was constructed as shown in Fig. 3, with two parallel branches modelling the two different vascular responses, dilation and constriction. A third-order linear time-invariant model for each branch was sufficient to prevent oscillations in the output. A pure transport delay was included in the model to reflect the lag in the haemodynamic response to stimulation. We refer to this model as the D–C (dilation–constriction) model throughout the article. The model has nine parameters, four for each component, with the time delay as an additional parameter. Laplace transforms were used as a convenient representation of linear time-invariant systems. However, the relationship between the CSD input and the CBF output can also be written as a set of ordinary differential equations as follows:

$$\begin{aligned} &\dddot{y}_d(t)+a_1\ddot{y}_d(t)+b_1\dot{y}_d(t)+c_1 = K_1c_1u(t), \quad && y_d(0)=\dot{y}_d(0)=\ddot{y}_d(0)=0\\ &\dddot{y}_c(t)+a_2\ddot{y}_c(t)+b_2\dot{y}_c(t)+c_2 = K_2c_2u(t), \quad && y_c(0)=\dot{y}_c(0)=\ddot{y}_c(0)=0\\ &f(t+\tau) = y_d(t)-y_c(t) \end{aligned} \tag{1}$$

where $u(t)$ denotes the CSD input, $f(t)$ denotes the CBF output, and $y_d(t)$ and $y_c(t)$ are the state variables representing the dilation and the constriction components, respectively. The parameter $\tau$ is a constant representing the time delay within the system. All the initial conditions used in solving the above differential equations are zero.

Importantly from the above linear differential equations, it is possible to formally derive the CBF impulse response functions (IRFs) (see Appendix B) under all experimental conditions. The major assumption in such model-based approach is that the identified model can adequately fit experimental data under these conditions.

Once the structure of the model is identified, the model-based method for IRF estimation has a considerable advantage over the data-driven deconvolution method for identifying the IRFs (Ances et al., 2000; Li and Freeman, 2007; Martindale et al., 2005), as the latter is much more vulnerable to the measurement and physiological noise present in the data.

Concurrent electrophysiological data (in terms of the modified CSD pulse trains) and the LDF data collected under paradigm 1 were used to test the goodness-of-fit of the model under three different durations of stimulation (2, 8, and 16 s), and for seven different IBSIs (0.6, 1, 2, 3, 4, 6, and 8 s). Parameter optimisation was carried out using a nonlinear least squares algorithm (Levenberg–Marquardt algorithm, Matlab (v7.3.0) function "lsqnonlin"). The differential equations were solved by first writing them in the state space form:

$$\begin{bmatrix}\dot{x}_1(t)\\ \dot{x}_2(t)\\ \dot{x}_3(t)\end{bmatrix} = \begin{bmatrix}0 & 1 & 0\\ 0 & 0 & 1\\ -c_1 & -b_1 & -a_1\end{bmatrix}\begin{bmatrix}x_1(t)\\ x_2(t)\\ x_3(t)\end{bmatrix} + \begin{bmatrix}0\\ 0\\ K_1c_1\end{bmatrix}u(t)$$

$$y_d(t) = [1 \quad 0 \quad 0]\begin{bmatrix}x_1(t)\\ x_2(t)\\ x_3(t)\end{bmatrix}$$

for the dilation component, and

$$\begin{bmatrix}\dot{x}_4(t)\\ \dot{x}_5(t)\\ \dot{x}_6(t)\end{bmatrix} = \begin{bmatrix}0 & 1 & 0\\ 0 & 0 & 1\\ -c_2 & -b_2 & -a_2\end{bmatrix}\begin{bmatrix}x_4(t)\\ x_5(t)\\ x_6(t)\end{bmatrix} + \begin{bmatrix}0\\ 0\\ K_2c_2\end{bmatrix}u(t)$$

$$y_c(t) = [1 \quad 0 \quad 0]\begin{bmatrix}x_4(t)\\ x_5(t)\\ x_6(t)\end{bmatrix}$$

for the constriction component. The variables $x_1$, $x_2$, $x_3$, $x_4$, $x_5$, $x_6$ are the state variables of the D–C model. The CBF time series can be written in terms of the six state variables as

$$f(t+\tau) = [1 \quad 0 \quad 0 \quad -1 \quad 0 \quad 0]\begin{bmatrix}x_1(t)\\ x_2(t)\\ x_3(t)\\ x_4(t)\\ x_5(t)\\ x_6(t)\end{bmatrix}$$

Then the Matlab function "ode113" was used to compute the CBF time series. The delay parameter $\tau$ was not included in the optimisation procedure. Instead it was determined by inspecting the averaged CBF time series (over all animals and all trials) within the first second of stimulus onset. Once determined, the time series of CBF data were simply shifted back in time by $\tau$ prior to model parameter optimisation. The exact value for $\tau$ is not crucial to the results of the parameter optimisation. Thus we have eight model parameters to optimise for each data set. Potentially, 21 sets of model parameters can be obtained each optimised under the 21 different stimulus types. We shall show below that the model can adequately capture the whole range of the stimulation paradigms with five of the eight parameters being clamped and only three parameters to refine the fit.

*Investigating the possibility of finding a single set of model parameters*

We investigated the possibility of using a single set of model parameters to fit the CBF responses for the 21 trial types. If a single model parameter set could provide satisfactory fits to our data over all conditions, it would indicate that as far as our data are concerned, the relationship between the neural signal (CSD) and the haemodynamic signal (CBF) is linear under our experimental conditions. In order to find such parameter set, we calculated the IRF for each stimulus type, and as they were similar in terms of the height and width of the response pulses (see the Results section), we then averaged the IRFs over for the 2-, 8-, and 16-s conditions, respectively. We subsequently identified three sets of corresponding model parameters ($\theta_2$, $\theta_8$, and $\theta_{16}$) using the three mean IRFs as the outputs of the D–C model, with the input being a unit impulse at time zero. These three parameter sets were used over all stimulus types to compare their performances in fitting the CBF responses. The normalised sum of squares of errors (nSSE) was calculated from

$$\text{nSSE} = \frac{\sum_{i=1}^{N}\left(f_i - \hat{f}_i\right)^2}{N-p} \tag{2}$$

where $f_i$ and $\hat{f}_i$ were the measured and fitted CBF data, respectively, $p$ was the number of parameters fitted, and $N$ was the number of data points, as the data lengths used for the 2-, 8-, and 16-s conditions were different. Comparison of the nSSE values enabled us to select the 'optimal' model parameter set that could be used to fit the CBF responses over all conditions.

*Ineorporating flexibility in the D–C model.* Although a single model parameter set could be used to fit the CBF responses, the fits were not uniformly good, with the goodness-of-fit values ($R^2$) ranging from 0.78 to 0.98. This is not surprising given the huge variations in our data between both sessions and animals.

To further improve the performance of the model without having to optimise all model parameters, we explored the possibility of allowing a subset of the eight model parameters to be optimised. This was done by searching for commonalities and differences in the model's dynamic characteristics generated by the three sets of model parameters $\theta_2$, $\theta_8$, and $\theta_{16}$. With the structure of the model predefined, the overall model dynamics were solely dependent on the component dynamics, which was closely related to the poles (i.e., the three roots in the denominator) of the two transfer functions representing

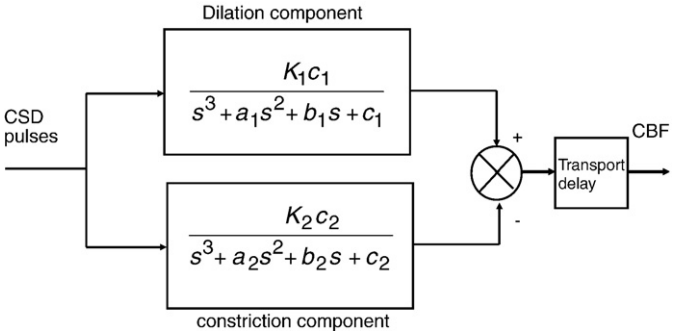


**Fig. 3.** The block diagram of a linear time-invariant dynamic model relating neural activity (the CSD pulse train) to the CBF time series. The two branches of the model represent the dilation (top branch) and the constriction component (bottom branch), respectively. The ordinary differential equations relating the input and the output of the model are written in Laplace transform, a standard frequency domain representation of linear time-invariant systems. The model has nine parameters including the transport delay. The transport delay was determined manually by inspection of the averaged CBF time series. Hence, eight model parameters need to be optimised.

dilation and constriction. Specifically, if all three poles for each of the third order system were real and negative (for stable models), the inverse of the values of the poles would be the three time constants associated with the system. The larger the magnitude of the poles, the faster would be the dynamics of the system. On the other hand, if two of the poles were complex conjugate to each other, then the inverse of the real part of the poles would determine the time constant, while the imaginary part would be associated with the degree of oscillation present in the system. The larger the magnitude of the imaginary part, the more oscillatory would be the system (Raven, 1968). Appendix B provides a derivation of the impulse response function of a canonical third order linear dynamic system.

Based on the above properties of transfer functions, we superimposed the poles of the dilation and constriction components of the three models in the complex plane. From the locations of the poles, we were able to determine commonalities and discrepancies across different stimulus conditions and select model parameters that could be adjusted in an optimisation process to improve the goodness-of-fit of the model over all stimulus conditions. This process enabled us to clamp five of the eight model parameters at their optimal values, while allowing three model parameters to be reoptimised for each data set to refine model fit under each stimulus condition.

### *Model validation*

The D–C model and the parameter optimisation strategy were tested using data sets collected from different animals using a completely different experimental paradigm. Experimental paradigm 1 was used to estimate a basic set of optimal model parameters, and experimental paradigm 2 was used to evaluate the performance of the optimal parameter set and the effectiveness of the optimisation strategy.

## Results

### *Simulation*

Two time series $y_1(t)$ and $y_2(t)$ were generated using Eqs. (A1) and (A2), respectively (see Appendix A). The variable $K$ in Eq. (A2) was set to four different values: 0.25, 0.2, 0.15, and 0.1. The corresponding gains of the system defined by Eq. (A2) are therefore 0.53, 0.42, 0.32, and 0.21, respectively. The subtraction of the two time series $y_1(t)$–$y_2(t)$ was then calculated for each $K$, and they are shown as solid traces in Figs. 4(a)–(d), superimposed with the two time series $y_1(t)$ (dashed) and $y_2(t)$ (dotted).

It can be seen that when $K$ is relatively high (Fig. 4(a)), the time series $y_1(t)$–$y_2(t)$ has an initial overshoot followed by an ascending ramp during stimulus onset period; during stimulus cessation, it decreases rapidly initially, followed by a slight increase before it returns to baseline slowly. The time course is very similar to our data shown in Fig. 2(c) (without the response to the probing block). As $K$ decreases, the overshoot characteristic disappears, so does the transient increase during the phase of stimulus cessation.

This simulation demonstrates that the complex characteristics of the haemodynamic responses can be generated by two slightly different 'bump' functions subtracting from each other, rather like two different forces acting in the opposite direction. By varying the relative contributions of the two time series and then subtracting them, we have generated a range of time series with temporal characteristics very similar to the various haemodynamic responses published in the literature. This simulation lands support to our hypothesis that neurovascular coupling may be modelled by two components representing vasodilation and vasoconstriction, respectively, with a model structure shown in Fig. 3. It is important to note that the two 'bump' functions were generated by two linear time-invariant dynamic models, respectively.

### *Model parameter estimation*

The proposed linear dynamic model of the neurovascular coupling has four model parameters for each component, and a transport delay parameter $\tau$. Visual inspection of the first second of the mean CBF time series over all conditions and subjects suggested that the value of this parameter $\tau$ was around 0.3 s. A variation of $\pm 0.1$ s in this delay parameter did not produce significantly different results to the model fittings. The model was optimised for each of the 21 stimulus conditions, with neural signal being the modified CSD pulse trains, shown in Fig. 5(a). Fig. 5(b) shows the transient characteristics of the CSD profile for the first 2 s of the stimulus onset, in particular the neural adaptation to pulse of the stimulus train immediately after stimulus onset was much stronger than that of the 'steady-state' adaptation reached at a later time point during stimulus presentation. The model fittings of CBF, shown in Fig. 6 as black dashed traces, compared well with the measured CBF data (solid dark grey) across all conditions. The light grey band in each subplot is $\pm 1$ SD of the data over 11 subjects. It can be seen that variations between individual subjects are large. However, the D–C model was able to fit well all individual subject CBF time series over all conditions (see supplemental Figure S1 for the model performance under a representative condition for all 11 subjects).

The results demonstrated that a linear dynamic model was capable of capturing not only the temporal dynamics of the CBF responses with respect to the conditioning block of stimulus with durations up to 16 s but also the CBF responses to the probing block of stimulus, which were applied within the CBF return-to-baseline period. Furthermore, the structure of the model was robust over a wide range of individual subject data.

### *Single optimal model parameter set*

Using the above 21 sets of model parameters, we computed the IRFs. Figs. 7(a), (b), and (c) shows the model fitted IRFs under 2-, 8-, and 16-s conditions, respectively. Each IRF within a subplot corresponds to a different IBSI. Fig. 7(d) shows the mean IRFs for 2-, 8-, and 16-s conditions superimposed with each other. What is evident is that the IRFs across all conditions have very similar peak values, latencies (time to peak), and full width at half maximum (FWHM) values. They all have undershoot and overshoot characteristics during the return-to-baseline phase. The major difference is the degree of magnitude of undershoot and overshoot and their timings during the return-to-baseline period. What is particularly noticeable is that under the 2-s conditions, the estimated IRFs were less robust in that they were more variable for the different IBSIs. This we believe is due to the disadvantaged signal-to-noise ratio from short stimulation and will be discussed in detail in the Discussion section.

The three mean IRFs were subsequently used to generate three sets of model parameters $\theta_2$, $\theta_8$, and $\theta_{16}$, whose values are listed in Table 1. The three models corresponding to these three parameters are referred to as $M_2$, $M_8$, and $M_{16}$, respectively. Each model was used to fit the CBF responses across all 21 stimulus types. The results are shown in the Supplemental Figures S2, S3, and S4. For each model, nSSE were calculated, and Fig. 8 shows the histogram of nSSE for the three models under the three conditions (2, 8, and 16 s) over the seven different IBSIs. As expected, model $M_2$ provided the best fits for stimulus with conditioning block of 2, but the nSSE values were significantly bigger for stimulus with conditioning block of 16. Similarly, model $M_8$ provided the best fit for stimulus with conditioning block of 8. It also predicted well for the 2-s conditions. But again it was not very good at predicting long duration stimulation data. Model $M_{16}$ fitted the 16-s data best, at the expense of slightly inferior predictions under the short stimulation conditions.

The above exercise highlighted the problem of using an estimated IRF from a short stimulus paradigm to predict the CBF response to a

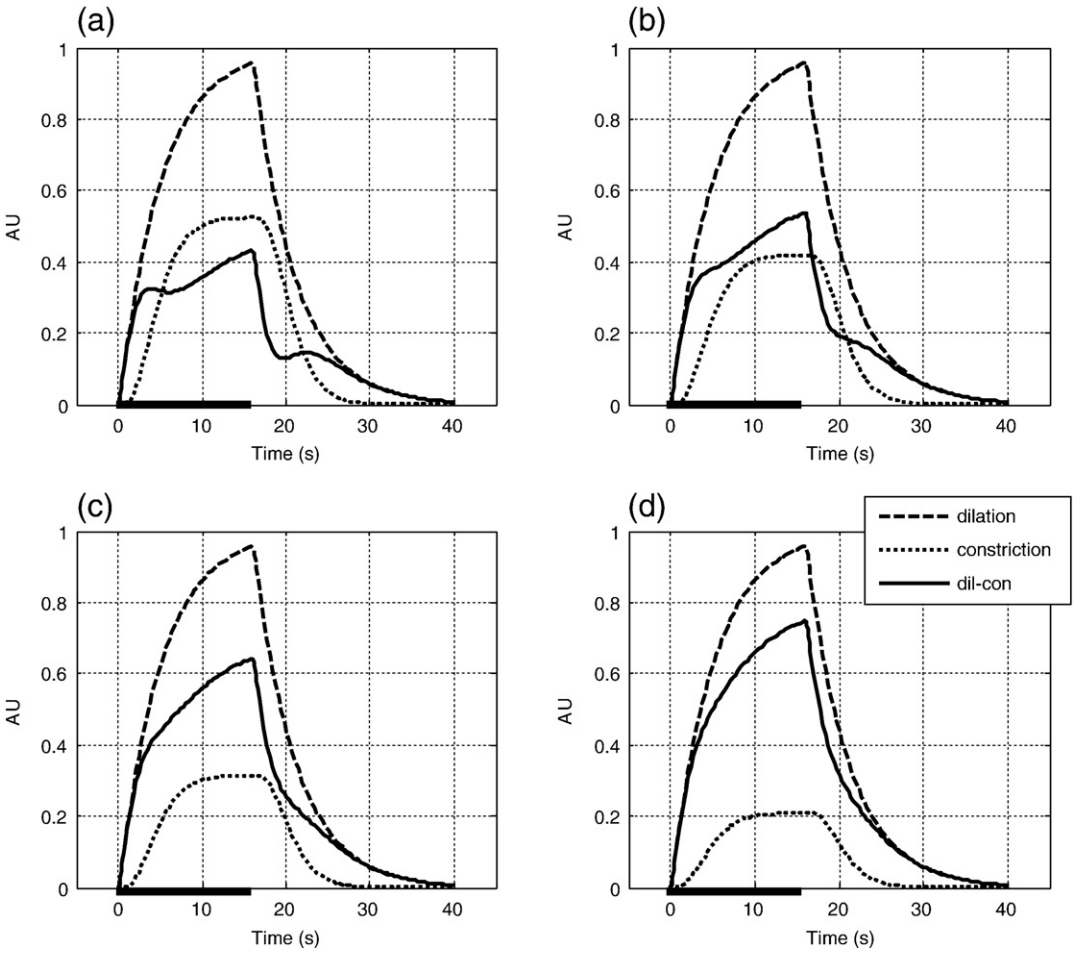


**Fig. 4.** Results of the proof-of-concept simulation of the CBF time series (solid curve) obtained from subtracting two time series slightly out of phase with each other. By keeping one time series (dashed curve) unchanged but decreasing the amplitude of the other time series (dotted curve), a range of CBF time series can be obtained with temporal characteristics similar to those published in the literature. Four examples are provided with the gain of the dotted time series set at (a) 0.53, (b) 0.42, (c) 0.32, and (d) 0.21, respectively. The gain of the dashed time series is unity. Black bars on the time axis indicate the duration of the stimulation (16 s).

long duration stimulus (Ances et al., 2000; Li and Freeman, 2007; Martindale et al., 2005). Figures S2, S3, and S4 showed that neither of the models $M_2$ and $M_8$ could adequately predict the temporal characteristics of the 16-s data during the onset period and the return-to-baseline phase during which a probing stimulus was applied. However, the model $M_{16}$ performed reasonably well across all stimulus conditions, indicating that the neurovascular coupling relationship maybe modelled by a linear dynamic system. We suggest that the failure of models $M_2$ and $M_8$ in predicting CBF responses to long duration stimuli did not necessarily imply that the underlying system was nonlinear. It could simply be that the IRFs under short stimulation paradigms were poorly estimated. This will be discussed further in the Discussion section.

Pair-wise *t*-tests were carried out on the nSSE values, and it was found that overall the model $M_2$ had significantly higher nSSE values compared with the other two models ($p<0.05$), and there was no significant difference in terms of the nSSE values between the models $M_8$ and $M_{16}$. As $M_{16}$ has a more robust performance across all stimulus conditions, it was decided to use the parameters $\theta_{16}$ as the 'optimal' model parameter set from which a subset of the parameters could be further optimised.

*Model parameters for fine tuning*

The poles of the three models $M_2$, $M_8$, and $M_{16}$ were calculated and are shown superimposed in Fig. 9, with subplots (a) and (b) being the locations (in the complex plane) of the poles of the dilation and constriction components, respectively.

For the dilation component, the locations of the poles of the three models are remarkably consistent. This suggests that the three dynamic model parameters ($a_1$, $b_1$, and $c_1$) associated with the dilation component are reasonably robust over stimulation duration.

However, there are some differences in the location of the poles for the constriction component over the three models, suggesting that the constriction parameters ($a_2$, $b_2$, and $c_2$) may vary for different stimulus durations. The parameter $a_2$ can be shown to be the sum of the real parts of the three poles of the constriction transfer function, and the parameters $b_2$ and $c_2$ are related to the imaginary parts of the complex poles (Appendix B). Looking closely at the predictions using $\theta_{16}$ on the short stimulation data (Supplemental Figure S4), it was evident that during the return-to-baseline phase, the predicted CBF had a slow but strong oscillatory component present whereas the measurement CBF was less oscillatory. This suggests that parameters $b_2$ and $c_2$ should be reoptimised to best fit the oscillatory characteristics in the data. We noticed further that certain trials show a mismatch between the measured and the predicted CBF during the onset period of stimulus, indicating that the gain of the model may need further tuning. As the gain of the overall model was given by the difference $K_1$–$K_2$, we decided to fine tune the gain of the constriction component $K_2$. Hence the three parameters $K_2$, $b_2$, and $c_2$ associated with the constriction model were reoptimised in order to improve the model fitting for each stimulus condition. The other five model parameters were clamped at their original values in $\theta_{16}$. The refined model fittings, after optimising three model parameters, compared well with the measured CBF time series over all 21 conditions (see

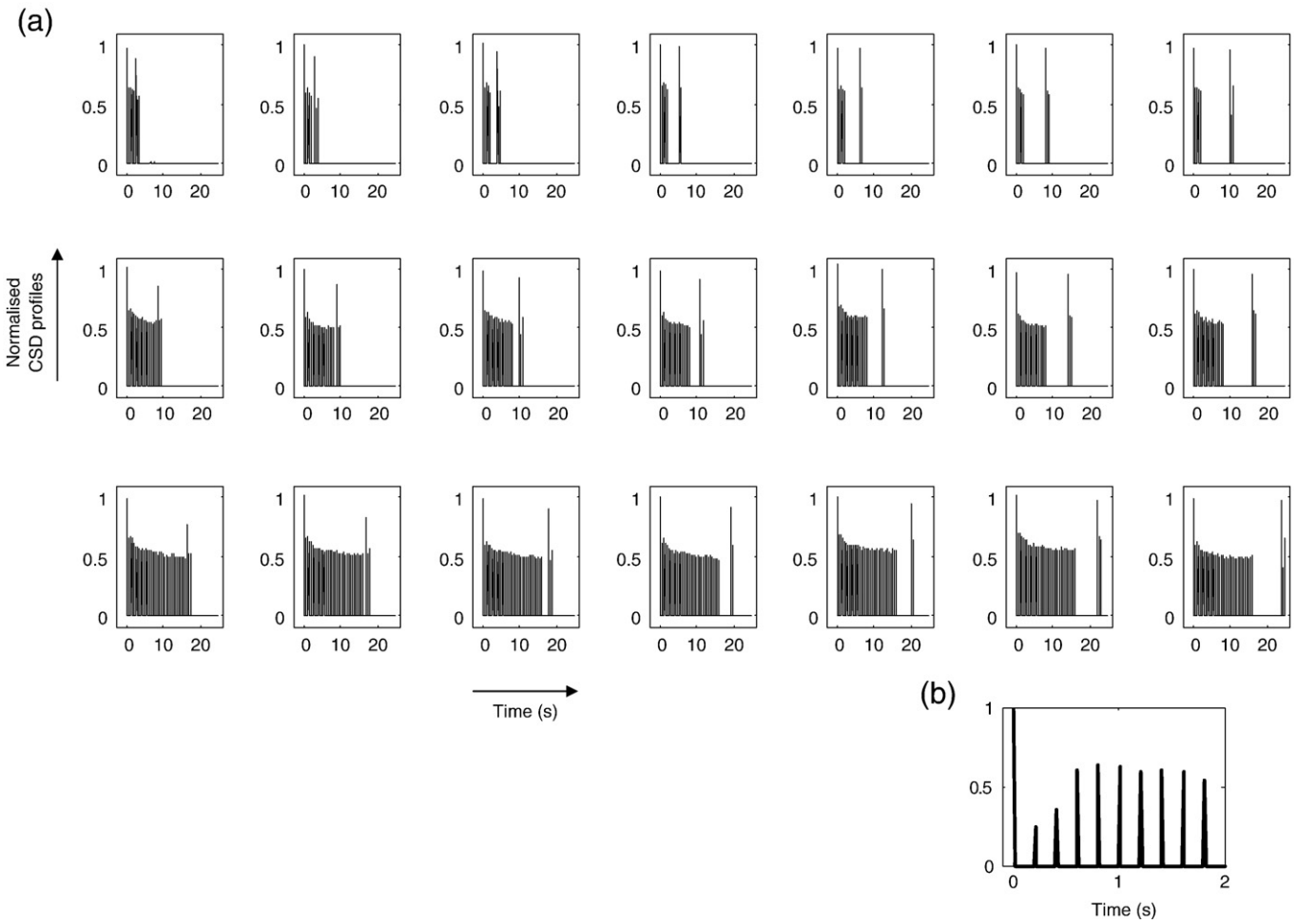


**Fig. 5.** (a) The mean CSD time series of all 21 trial types. They are used as inputs to the D–C model. (b) A zoomed-in plot of a representative CSD time series for the first 2 s of stimulation, showing neural adaptation characteristics.

supplemental Figure S5), and the results are very similar to those obtained by optimising all eight model parameters (Fig. 6). A pair-wise *t*-test to compare the nSSE (i.e., the error score) obtained using this method with the method in which all eight model parameters were optimised showed that there was no significant difference between the two methods ($p<0.05$). The values of the three model parameters after reoptimisation are also close to their original values, with a mean percentage change less than 5%.

*Model validation*

The D–C model was validated on the paradigm 2 data set obtained from five animals. The optimisation procedure used was the same as that outlined above: based on the parameter set $\theta_{16}$, the three parameters $K_2$, $b_2$, and $c_2$ associated with the constriction component were reoptimised for each stimulus type. The results are shown in Fig. 10, and the optimised parameter values are shown in Table 2. Despite the fact that the data were from different animals and from a different experimental protocol, it can be seen that there were only slight differences in the values of the three model parameters and only slight adjustments were necessary for the linear dynamic model to fit the changes in CBF under all four stimulus conditions using the corresponding CSD data.

## Discussion

The D–C model was at least in part motivated by the research implicating the neural control of the dilation and constriction of blood vessels, and this will be discussed below. However, the importance of the demonstration of the linearity of the system linking changes in neural activity to changes in CBF over a large dynamic range is that it allows the constrained generation of very different model structures that can be used as hypotheses of the physiological mechanisms of neurovascular coupling, which will be discussed below.

*Evidence for blood vessel dilation and constriction due to evoked neural activity*

Mechanisms coupling neural activity to blood flow have been extensively studies at the cellular level (see reviews by Hamel (2006) and Iadecola and Nedergaard (2007)). Current research suggests that astrocytes may play an important role in cerebrovascular regulation, specifically intracellular $Ca^+$ increases in astrocytic endfeet induce either vasodilation, or vasoconstriction, or both (Anderson and Nedergaard, 2003; Filosa and Blanco, 2007; Metea and Newman, 2006; Zonta et al., 2003). A recent *in vitro* study of the rat hippocampal slices (Gordon et al., 2008) showed that the level of $O_2$ concentration in tissue dictates how astrocytes control the vascular response to changes in neural activity. It was found that, in response to synaptic activation, the same arterioles dilated in conditions of low $O_2$ concentration (20%) but constricted in conditions of high $O_2$ concentration (95%). As many of functional studies have shown that evoked neural activity induces an initial decrease in local tissue oxygen tension before it is increased as the regional CBF increases (Bartlett et al., 2008; Thompson et al., 2004), the above *in vitro* work

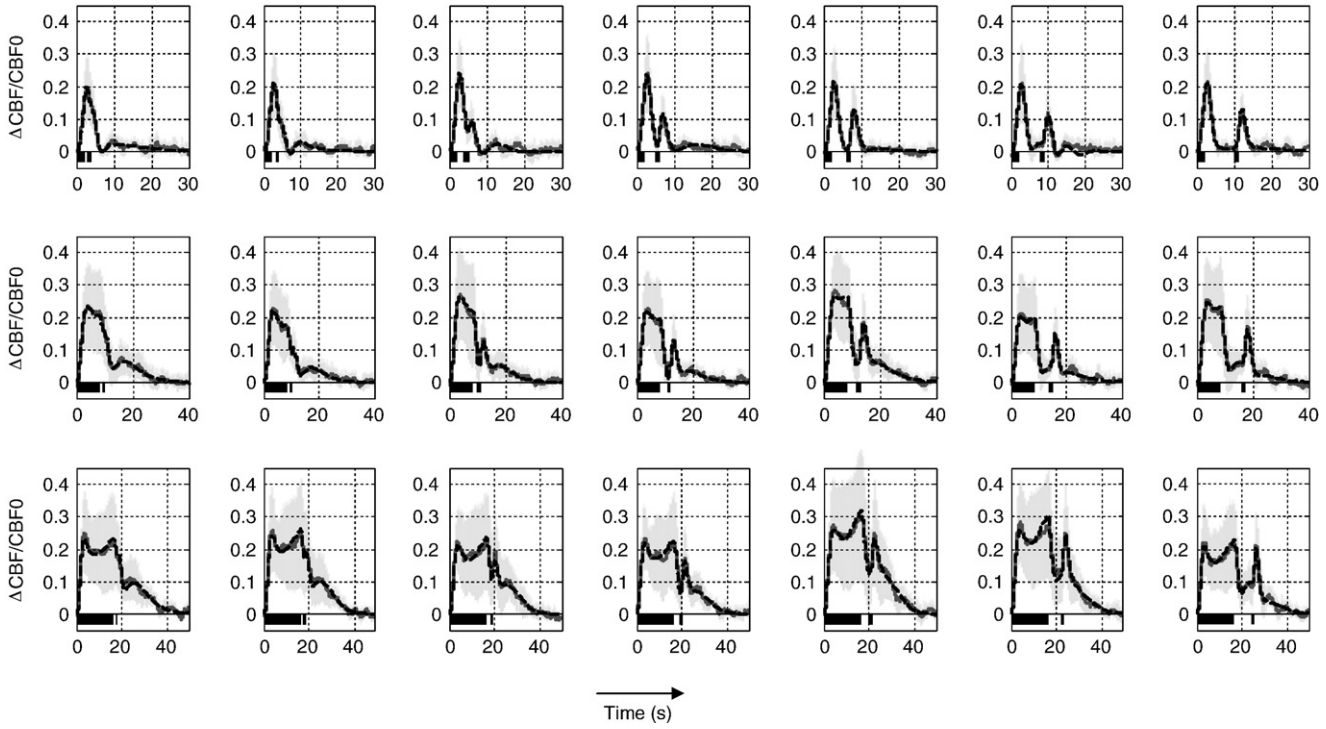


**Fig. 6.** Fitted fractional changes in CBF time series (black dashed curve) superimposed with the actual animal-and-trial-averaged CBF data (grey solid curve) ($n = 11$). The light grey band is $\pm 1$ standard deviation of the data. Black bars on the time axis indicate the duration of stimulation. For each of the 21 trial types, all eight model parameters were optimised.

offers some evidence for an initial tendency for blood vessels to dilate due to decreased $O_2$ concentration, followed by the tendency for the same vessels to constrict due to the subsequent increase in tissue $O_2$ concentration. However, it is unclear how the two interact with each other, resulting in the overall dilation of blood vessels evident in the experimental data.

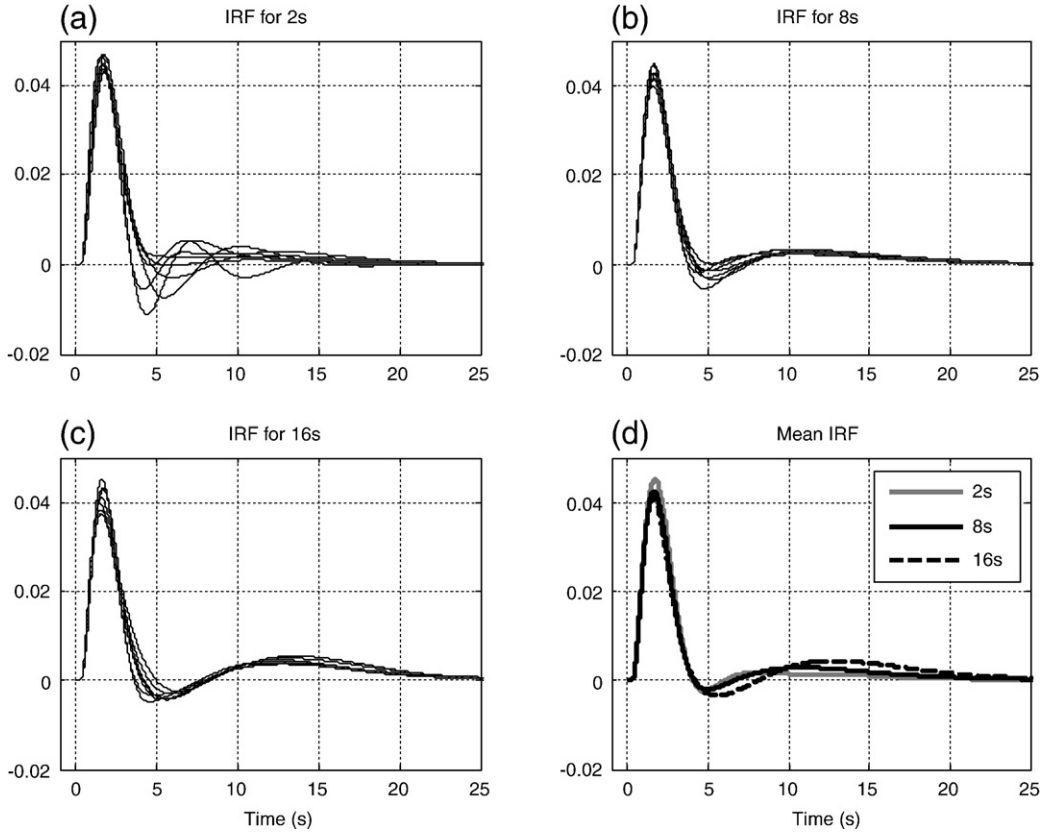


**Fig. 7.** Impulse response functions (IRF) for (a) 2-s conditions, (b) 8-s conditions, and (c) 16-s conditions. Each plot has seven IRFs corresponding to the seven different IBSIs: 0.6, 1, 2, 3, 4, 6, and 8 s. (d) The mean IRFs for the 2-s condition (grey solid), 8-s condition (black solid), and 16-s condition (black dashed), respectively.

**Table 1**
Eight optimised model parameters in paradigm 1, under 2-s stimulus duration conditions ($\theta_2$), 8-s stimulus duration conditions ($\theta_8$), and 16-s stimulus duration conditions ($\theta_{16}$).

| | K1 | a1 | b1 | c1 | K2 | a2 | b2 | c2 |
|---|---|---|---|---|---|---|---|---|
| $\theta_2$ | 29.0 | 2.61 | 4.14 | 0.93 | 19.9 | 1.56 | 1.13 | 0.23 |
| $\theta_8$ | 30.3 | 2.88 | 4.70 | 0.91 | 20.7 | 1.54 | 0.99 | 0.19 |
| $\theta_{16}$ | 30.9 | 3.10 | 5.25 | 0.94 | 20.6 | 1.82 | 0.95 | 0.19 |

It is also possible that the overall observed CBF response was the result of a larger proportion of the local blood vessels dilating simultaneously with a smaller proportion of blood vessels constricting. This was observed by an *in vivo* study using two photon laser scanning microscopy (Stefanovic et al., 2007). The study found that electrical stimulation of the forepaw of rodents induced dilation in most blood vessels of diameter up to 30 μm, but a small proportion of blood vessels showed a decrease in their diameters. As the study only recorded steady-state vascular responses to sustained electrical stimulation, the temporal characteristics of the dilating and constricting blood vessels were not available.

Although most studies found that changes in neural activity induce changes in the regional blood flow, a recent study (Sirotin and Das, 2009) observed a decoupling between neural activity and the CBF. More specifically, a change in CBF was measured with no measurable change in the local field potentials. Although the work raises the question of consistency of neurovascular coupling, more research is needed to replicate such findings and to investigate under what experimental conditions such decoupling may be likely to occur. More importantly neurovascular coupling as a phenomenon is not invalidated by such findings; and the scientific effort in searching for the underlying mechanism will continue.

*A linear dynamic coupling*

If a system is linear time-invariant, it is completely characterised by its IRF. For this reason, IRFs have been used to test the linearity or otherwise of the underlying system governing changes in neural activity and the ensuing changes in CBF. Previous studies (Ances et al., 2000; Martindale et al., 2005) suggested that this relationship was nonlinear with respect to stimulus duration. In these studies, the estimated IRFs, from experiments with short stimulus duration, were used to predict the CBF time series obtained from experiments with longer stimulus durations. The conclusion of nonlinearity was drawn from the fact that the predicted CBF time series failed to match the measured data satisfactorily.

Our results highlighted the fact that the estimated IRFs using short duration data were less consistent over the different IBSIs compared with those using longer duration data (Fig. 7). This is mainly due to two reasons. One is that the evoked CBF time series for brief stimulus generally have smaller amplitude than those with longer duration stimulus. As a result, the signal-to-noise ratio of the data obtained from short duration experiments is not as good as that from long duration experiments. Secondly, the temporal characteristics of the CBF IRF during the return-to-baseline period is complex, involving both undershoot as well as overshoot of the response from its baseline condition. For CBF data with short duration stimulus, these characteristics are largely buried in the baseline noise of the CBF responses. However, for long-duration stimulation data, these characteristics are reflected in the CBF time series during the onset period of stimulation, and the IRFs can be estimated more accurately. Hence the poor predictive power using estimated CBF IRFs demonstrated by previous studies could be due to poor estimates of these IRFs rather than the underlying system being nonlinear.

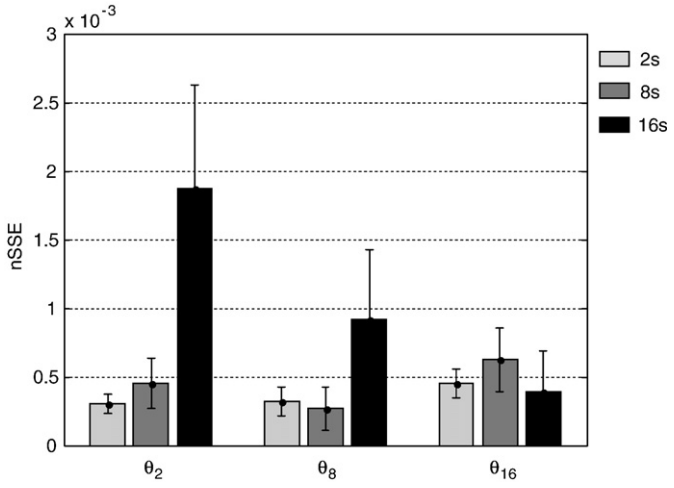


**Fig. 8.** Comparison of the normalised sum of squares of errors (nSSE). Each of the three model parameter set $\theta_2$, $\theta_8$, and $\theta_{16}$ was used to fit the CBF time series over all stimulation conditions. Each bar represents the mean nSSE over the seven IBSIs for the 2-s condition (light grey), 8-s condition (dark grey), and 16-s condition (black). The error bar represents $\pm 1$ standard deviation of the data.

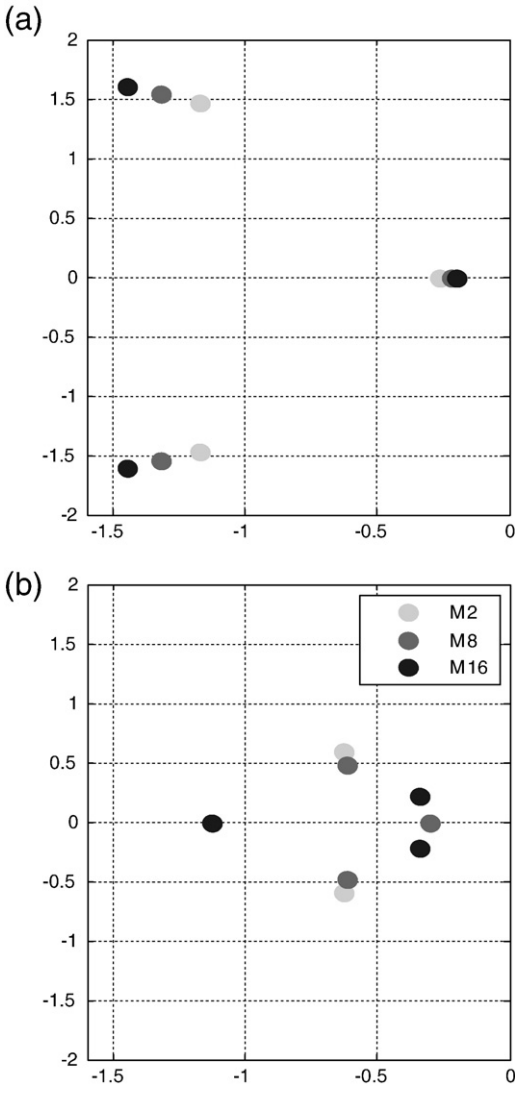


**Fig. 9.** The pole locations of the transfer function in the complex plane for (a) the dilation component and (b) the constriction component. The pole locations for models $M_2$, $M_8$, and $M_{16}$ are plotted as light grey dots, dark grey dots, and black dots, respectively. For the dilation component, the locations of the poles do not vary significantly. For the constriction component, the locations of the poles for $M_{16}$ are very different from those for $M_2$ and $M_8$.

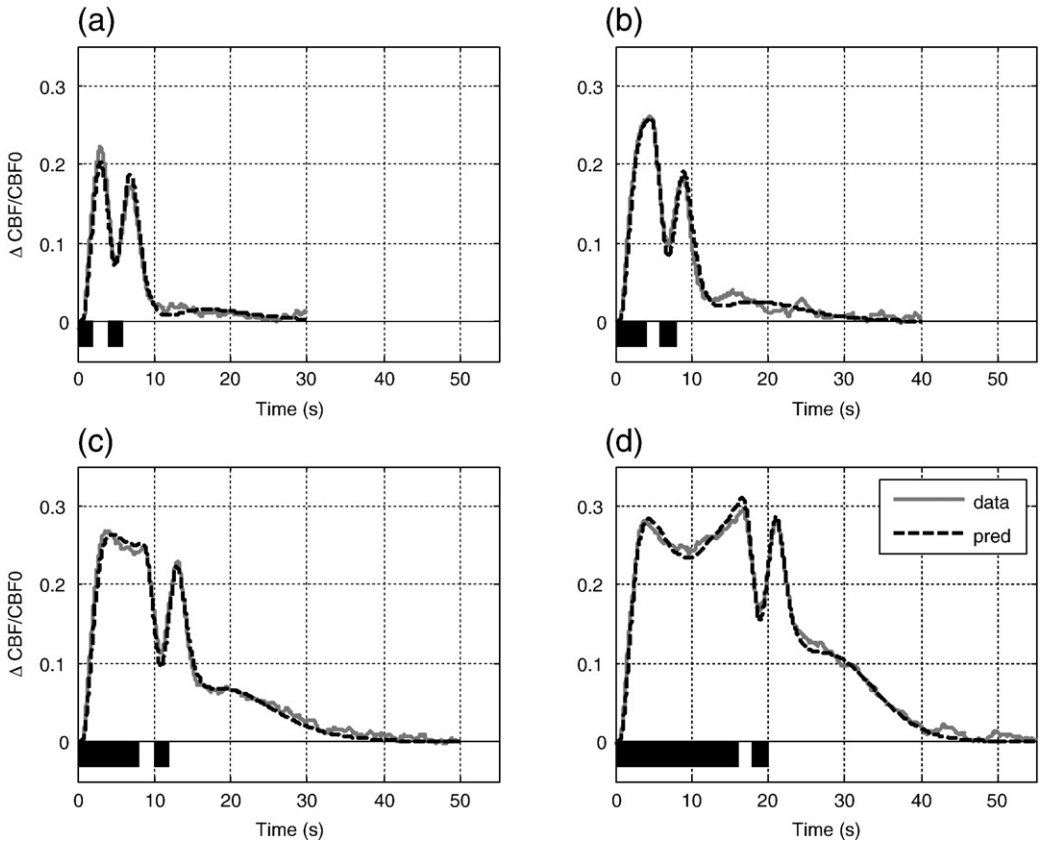


**Fig. 10.** Results of model validation using paradigm 2 data. The fitted fractional changes in CBF time series (black dashed) are superimposed with the animal-and trial-averaged data (grey solid) over 5 subjects. Conditioning block stimulus duration varies from (a) 2, (b) 4, (c) 8, and (d) 16 s. The probing block duration is fixed at 2 s, with the IBSI fixed at 2 s. Black bars on the time axis indicate the duration of stimulation.

We have demonstrated that, for our data and applying model-based approach, a single CBF IRF (obtained from the 16-s stimulation conditions) could be used to fit the CBF time series over stimulus durations 2–16 s, and over inter-block-stimulus intervals 0.6–8 s. This finding suggests that the neurovascular coupling linking the CSD pulses and the CBF time series is potentially linear over stimulus duration. As neurovascular coupling plays an important part in the coupling of neural activity to the fMRI BOLD signal, the finding of linearity of neurovascular coupling has important implications on the analysis and interpretation of the BOLD signal.

An important implication of linearity is that the structure of the D–C model can be formally manipulated into different structural configurations, which can be used as hypotheses in the search of the coupling of the underlying dilation and the constriction processes.

*Alternative model structures*

The D–C model presented in this article assumed that the source of both blood vessel dilation and constriction was of neural origin, hence both components were driven by the CSD signal. However, another source of vessel constriction is auto-regulation (Johnson, 1986; Kontos, 1981). This refers to the intrinsic ability of cerebral blood vessels to dilate or constrict to maintain adequate blood flow and hence supply of oxygen to the brain. Under the framework of linearity, it is possible to explore such model structure by assigning the input of the constriction component to be the haemodynamic response, thus forming a feedback loop in the model. Alternatively the interplay between cerebral auto-regulation and functional hyperaemia could be investigated by feeding both neural and haemodynamic signals to the constriction element.

Another possible model structure for neurovascular coupling is to have vasodilation and constriction to be driven by different components in the neural responses, with dilation driven by the short-latency temporal sink, and constriction driven by the long-latency temporal source in the CSD signal. This model is based on the fact that the short-latency temporal sink represents the excitatory post-synaptic potential (EPSP) whereas the long-latency temporal source represents the inhibitory post-synaptic potential (IPSP). The hypothesis is that EPSP is the source of vasodilation, and IPSP is the source for vasoconstriction. The haemodynamic response is the result of the interaction between EPSP and IPSP (Barth et al., 1993; Di et al., 1990). This theory may potentially explain the negative BOLD phenomena often observed in the regions surrounding the area of increased CBF (Devor et al., 2007; Kennerley et al., 2008). This is currently an active area of research.

Ultimately the structure of the model must be guided by physiological constraints and experimental data; however, the robustness of the estimated model parameters should provide insight into the likelihood of the model structure of neurovascular coupling.

*Other considerations*

Although our results suggest a linear dynamic model of neuro-vascular coupling with respect to stimulus duration of up to 16 s, it is

**Table 2**
Three of the eight model parameters were optimised in paradigm 2, under 2-, 4-, 8-, and16-s stimulus duration conditions.

| | K2 | b2 | c2 |
|---|---|---|---|
| 2 s | 20.2 | 1.00 | 0.16 |
| 4 s | 19.2 | 0.93 | 0.15 |
| 8 s | 18.1 | 0.93 | 0.17 |
| 16 s | 17.8 | 0.73 | 0.16 |

important to note that nonlinearity may become prominent if the duration of stimulation is much longer (Rasmussen et al., 2009). It has also been shown that neurovascular coupling with respect to stimulus intensity was nonlinear with saturation at higher stimulus intensities and with a dead-zone effect at lower stimulus intensities (Hewson-Stoate et al., 2005; Jones et al., 2004; Ureshi et al., 2005). Furthermore, stimulation frequency is also an important parameter in determining the relationship between neural activity and the evoked CBF responses, with wide-ranging conclusions about the nature of its influence on neurovascular coupling (Hewson-Stoate et al., 2005; Martindale et al., 2003; Nielsen and Lauritzen, 2001; Rasmussen et al., 2009). As most of these studies focused on the steady state rather than dynamic relationships, their conclusions may or may not extend to the dynamic coupling of neural activity and CBF responses. Thus the D–C model needs further evaluation using different stimulus frequencies, intensities, and durations. In the mean time as neurovascular coupling is an integral part of understanding the fMRI BOLD signal, it is being incorporated into a multi-compartment model (Zheng et al., 2005) to provide better interpretations of the BOLD signal and of the underlying neural activity.

## Conclusion

We have demonstrated that a linear dynamic model can adequately describe the relationship between neural activity and changes in CBF across blocks of different durations of (2–16 s) stimulation with different gaps (IBSIs) between them (0.6–8 s). The structure of the model can be interpreted in the framework of balance between blood vessel dilation and constriction.

An important result of our study is the demonstration that the neurovascular coupling is potentially linear dynamic. This result may impact on two fronts: one is that within the frame work of linearity, we can manipulate the structure of the model to investigate the possible sources of vasodilation and vasoconstriction; the other is in the analysis and modelling of the BOLD signals obtained in fMRI studies. It is to be hoped that our model will help the neurosurgeon/scientist in the interpretation of these signals in terms of the underlying neural activity and their interactions.

## Acknowledgments

The authors would like to thank the technical staff Mrs. M Simkins, Mr. M Port, Mrs. N Kennerley, and Mr. L Hetherington for their assistance. The work was supported by the Engineering and Physical Science Research Council grant: EP/D001218, the National Institute of Health grant: ROI-NS44567-01 and the Medical Research Council Coop group grant: 9825307.

## Appendix A. A proof-of-concept simulation

To demonstrate that the complex temporal characteristics of CBF maybe the result of two opposing processes acting upon blood vessels, two time series $y_1(t)$ and $y_2(t)$ were generated using two linear dynamic systems driven by a continuous square pulse lasting for 16 s. The first linear system has the transfer function

$$G_1(s) = \frac{2}{(s+10)(s+0.2)} \tag{A1}$$

and the second linear system has the transfer function

$$G_2(s) = \frac{K}{(s+1.1)(s+0.9)(s+0.8)(s+0.6)}. \tag{A2}$$

The two systems were selected loosely with the following criteria: (i) the first system is faster dynamically compare to the second system, and it has a gain of unity; and (ii) the second system is more delayed than the first system, and it has a variable gain reflected by the variable $K$. The two time series were then subtracted from each other and the temporal characteristics of the resultant signal $y_1(t)$–$y_2(t)$ were compared with the observed time series of CBF.

## Appendix B. Impulse response functions for linear dynamic systems

Consider the $n$th-order canonical linear dynamic system with the transfer function

$$G(s) = \frac{Ka_n}{s^n + a_1 s^{n-1} + \cdots + a_n} = \frac{K_1}{s-r_1} + \frac{K_2}{s-r_2} + \cdots \frac{K_2}{s-r_n}.$$

The impulse response function of the system is given by

$$IRF = f(t) = K_1 e^{r_1 t} + K_2 e^{r_2 t} + \cdots K_n e^{r_n t}.$$

If $r_1$ and $r_2$ are complex, written as $r_1, r_2 = R \pm jI$, then the impulse response function can be re-written as

$$f(t) = K_{12} e^{Rt} \sin(It + \alpha) + \cdots + K_n e^{r_n t}.$$

In the case of a canonical third-order linear dynamic system with the transfer function

$$G(s) = \frac{K_c}{s^3 + as^2 + bs + c} = \frac{K_c}{(s+p_1) + (s+p_2)(s+p_3)}$$

if it has a pair of complex conjugate roots $p_1, p_2 = \mathrm{R} \pm jI$, then its impulse response function is

$$f(t) = K_{12} e^{Rt} \sin(It + \alpha) + K_3 e^{p_3 t}.$$

Furthermore, the parameters $a$, $b$, and $c$ are related to the parameters $p_1$, $p_2$, and $p_3$ as

$$a = p_1 + p_2 + p_3, \quad b = p_1 p_2 + p_1 p_3 + p_2 p_3, \quad c = p_1 p_2 p_3.$$

If $p_1$ and $p_2$ are complex conjugate, then

$$a = 2R + p_3, \quad a = R^2 + I^2 + 2Rp_3, \quad c = \left(R^2 + I^2\right) p_3.$$

Note that parameter $a$ is independent of the imaginary part $I$ of the roots.

## Appendix C. Supplementary data

Supplementary data associated with this article can be found, in the online version, at doi:10.1016/j.neuroimage.2010.01.102.

## References

Ances, B.M., Zarahn, E., Greenberg, J.H., Detre, J.A., 2000. Coupling of neural activation to blood flow in the somatosensory cortex of rats is time-intensity separable, but not linear. J. Cereb. Blood Flow Metab. 20, 921–930.

Anderson, C.M., Nedergaard, M., 2003. Astrocyte-mediated control of cerebral microcirculation. Trends Neurosci. 26, 340–344.

Aubert, A., Costalat, R., 2002. A model of the coupling between brain electrical activity, metabolism, and hemodynamics: application to the interpretation of functional neuroimaging. NeuroImage 17, 1162–1181.

Barth, D.S., Kithas, J., Di, S., 1993. Anatomic organization of evoked potentials in rat parietotemporal cortex: somatosensory and auditory responses. J. Neurophysiol. 69, 1837–1849.

Bartlett, K., Saka, M., Jones, M., 2008. Polarographic electrode measures of cerebral tissue oxygenation: implications for functional brain imaging. Sensors 8, 7649–7670.

Bennett, M.R., Farnell, L., Gibson, W.G., 2008. Origins of blood volume change due to glutamatergic synaptic activity at astrocytes abutting on arteriolar smooth muscle cells. J. Theor. Biol. 250, 172–185.
Berwick, J., Johnston, D., Jones, M., Martindale, J., Redgrave, P., McLoughlin, N., Schiessl, I., Mayhew, J.E.W., 2005. Neurovascular coupling investigated with two-dimensional optical imaging spectroscopy in rat whisker barrel cortex. Eur. J. Neurosci. 22, 1655–1666.
Blockley, N.P., Francis, S.T., Gowland, P.A., 2009. Perturbation of the BOLD response by a contrast agent and interpretation through a modified balloon model. NeuroImage 48, 84–93.
Buxton, R.B., Uludag, K., Dubowitz, D.J., Liu, T.T., 2004. Modeling the hemodynamic response to brain activation. NeuroImage 23, S220–S233.
Devor, A., Tian, P.F., Nishimura, N., Teng, I.C., Hillman, E.M.C., Narayanan, S.N., Ulbert, I., Boas, D.A., Kleinfeld, D., Dale, A.M., 2007. Suppressed neuronal activity and concurrent arteriolar vasoconstriction may explain negative blood oxygenation level-dependent signal. J. Neurosci. 27, 4452–4459.
Di, S., Baumgartner, C., Barth, D.S., 1990. Laminar analysis of extracellular field potentials in rat vibrissa/barrel cortex. J. Neurophysiol. 63, 832–840.
Filosa, J.A., Blanco, V.M., 2007. Neurovascular coupling in the mammalian brain. Exp. Physiol. 92, 641–646.
Friston, K.J., Mechelli, A., Turner, R., Price, C.J., 2000. Nonlinear responses in fMRI: the balloon model, volterra kernels, and other hemodynamics. NeuroImage 12, 466–477.
Gerrits, R.J., Raczynski, C., Greene, A.S., Stein, E.A., 2000. Regional cerebral blood flow responses to variable frequency whisker stimulation: an autoradiographic analysis. Brain Res. 864, 205–212.
Gordon, G.R.J., Choi, H.B., Rungta, R.L., Ellis-Davies, G.C.R., MacVicar, B.A., 2008. Brain metabolism dictates the polarity of astrocyte control over arterioles. Nature 456, 745–749.
Hamel, E., 2006. Perivascular nerves and the regulation of cerebrovascular tone. J. Appl. Physiol. 100, 1059–1064.
Herman, P., Sanganahalli, B.G., Hyder, F., 2008. Multimodal measurements of blood plasma and red blood cell volumes during functional brain activation. J. Cereb. Blood Flow Metab. 29, 19–24.
Hewson-Stoate, N., Jones, M., Martindale, J., Berwick, J., Mayhew, J., 2005. Further nonlinearities in neurovascular coupling in rodent barrel cortex. NeuroImage 24, 565–574.
Huettel, S.A., McCarthy, G., 2001. Regional differences in the refractory period of the hemodynamic response: an event-related fMRI study. NeuroImage 14, 967–976.
Iadecola, C., Nedergaard, M., 2007. Glial regulation of the cerebral microvasculature. Nature Neuroscience 10, 1369–1376.
Johnson, P.C., 1986. Autoregulation of blood flow. Circ. Res. 59, 483–495.
Jones, M., Berwick, J., Mayhew, J., 2002. Changes in blood flow, oxygenation, and volume following extended stimulation of rodent barrel cortex. NeuroImage 15, 474–487.
Jones, M., Hewson-Stoate, N., Martindale, J., Redgrave, P., Mayhew, J., 2004. Nonlinear coupling of neural activity and CBF in rodent barrel cortex. NeuroImage 22, 956–965.
Kennerley, A.J., Berwick, J., Martindale, J., Johnston, D., Papadakis, N., Mayhew, J., 2005. Concurrent fMRI and optical measures for the investigation of the hemodynamic response function. MRM 54, 354–365.
Kennerley, A., Boorman, L., Johnston, D., Zheng, Y., Redgrave, P., Mayhew, J., Berwick, J., 2008. The Negative BOLD Effect in the Rodent Barrel Cortex Model: Investigation Using Multimodal Imaging and Electrophysiology. ISMRM, Abstract No. 222, Toronto, Canada.
Kida, I., Rothman, D.L., Hyder, F., 2007. Dynamics of changes in blood flow, volume, and oxygenation: implications for dynamic functional magnetic resonance imaging calibration. J. Cereb. Blood Flow Metab. 27, 690–696.
Kontos, H.A., 1981. Regulation of the cerebral-circulation. Annu. Rev. Physiol. 43, 397–407.
Lauritzen, M., 2001. Relationship of spikes, synaptic activity, and local changes of cerebral blood flow. J. Cereb. Blood Flow Metab. 21, 1367–1383.
Li, B., Freeman, R.D., 2007. High-resolution neurometabolic coupling in the lateral geniculate nucleus. J. Neurosci. 27, 10223–10229.
Mandeville, J.B., Marota, J.J.A., Ayata, C., Zaharchuk, G., Moskowitz, M.A., Rosen, B.R., Weisskoff, R.M., 1999. Evidence of a cerebrovascular postarteriole windkessel with delayed compliance. J. Cereb. Blood Flow Metab. 19, 679–689.
Martin, C., Berwick, J., Kennerley, A., Zheng, Y., Mayhew, J., 2009. Spatiotemporal complexity in the haemodynamic response to somatosensory stimulation in the unanaesthetised rat. Brain 2009, Abstract 602, Chicago.
Martindale, J., Mayhew, J., Berwick, J., Jones, M., Martin, C., Johnston, D., Redgrave, P., Zheng, Y., 2003. The hemodynamic impulse response to a single neural event. J. Cereb. Blood Flow Metab. 23, 546–555.
Martindale, J., Berwick, J., Martin, C., Kong, Y.Z., Zheng, Y., Mayhew, J.E.W., 2005. Long duration stimuli and nonlinearities in the neural–haemodynamic coupling. J. Cereb. Blood Flow Metab. 25, 651–661.
Mathiesen, C., Caesar, K., Akgoren, N., Lauritzen, M., 1998. Modification of activity-dependent increases of cerebral blood flow by excitatory synaptic activity and spikes in rat cerebellar cortex. J. Physiol. (Lond.) 512, 555–566.
Mayhew, J.E.W., Askew, S., Zheng, Y., Porrill, J., Westby, G.W.M., Redgrave, P., Rector, D.M., Harper, R.M., 1996. Cerebral vasomotion: a 0.1-Hz oscillation in reflected light imaging of neural activity. NeuroImage 4, 183–193.
Metea, M.R., Newman, E.A., 2006. Glial cells dilate and constrict blood vessels: a mechanism of neurovascular coupling. J. Neurosci. 26, 2862–2870.
Mulligan, S.J., MacVicar, B.A., 2004. Calcium transients in astrocyte endfeet cause cerebrovascular constrictions. Nature 431, 195–199.
Nielsen, A.N., Lauritzen, M., 2001. Coupling and uncoupling of activity-dependent increases of neuronal activity and blood flow in rat somatosensory cortex. J. Physiol. 533, 773–785.
Nikos, K.L., 2002. The neural basis of the blood-oxygen-level-dependent functional magnetic resonance imaging signal. Phil. Trans. R. Soc. B 357, 1003–1037.
Nilsson, G.E., 1984. Signal processor for laser Doppler tissue flowmeters. Med. Biol. Eng. Comput. 22, 343–348.
Rasmussen, T., Holstein-Rathlou, N.-H., Lauritzen, M., 2009. Modeling neuro-vascular coupling in rat cerebellum: characterization of deviations from linearity. NeuroImage 45, 96–108.
Raven, F.H., 1968. Automatic Control Engineering. McGraw-Hill Book Company, Inc.
Riera, J.J., Watanabe, J., Kazuki, I., Naoki, M., Aubert, E., Ozaki, T., Kawashima, R., 2004. A state-space model of the hemodynamic approach: nonlinear filtering of BOLD signals. NeuroImage 21, 547–567.
Riera, J.J., Xiaohong, W., Juan Carlos, J., Ryuta, K., 2006. Nonlinear local electrovascular coupling. I: a theoretical model. Hum. Brain Mapp. 27, 896–914.
Riera, J.J., Jimenez, J.C., Wan, X., Kawashima, R., Ozaki, T., 2007. Nonlinear local electrovascular coupling. II: from data to neuronal masses. Hum. Brain Mapp. 28, 335–354.
Rosengarten, B., Lutz, H., Hossmann, K.A., 2003. A control system approach for evaluating somatosensory activation by laser-Doppler flowmetry in the rat cortex. J. Neurosci. Methods 130, 75–81.
Sheth, S.A., Nemoto, M., Guiou, M., Walker, M., Pouratian, N., Toga, A.W., 2004. Linear and nonlinear relationships between neuronal activity, oxygen metabolism, and hemodynamic responses. Neuron 42, 347–355.
Sirotin, Y.B., Das, A., 2009. Anticipatory haemodynamic signals in sensory cortex not predicted by local neuronal activity. Nature 457, 475–479.
Sotero, R.C., Trujillo-Barreto, N.J., 2007. Modelling the role of excitatory and inhibitory neuronal activity in the generation of the BOLD signal. NeuroImage 35, 149–165.
Sotero, R.C., Trujillo-Barreto, N.J., 2008. Biophysical model for integrating neuronal activity, EEG, fMRI and metabolism. NeuroImage 39, 290–309.
Stefanovic, B., Hutchinson, E., Yakovleva, V., Schram, V., Russell, J.T., Belluscio, L., Koretsky, A.P., Silva, A.C., 2007. Functional reactivity of cerebral capillaries. J. Cereb. Blood Flow Metab. 28, 961–972.
Thompson, J.K., Peterson, M.R., Freeman, R.D., 2004. High-resolution neurometabolic coupling revealed by focal activation of visual neurons. Nat. Neurosci. 7, 919–920.
Ureshi, M., Kershaw, J., Kanno, I., 2005. Nonlinear correlation between field potential and local cerebral blood flow in rat somatosensory cortex evoked by changing the stimulus current. Neurosci. Res. 51, 139–145.
Ureshi, M., Matsuura, T., Kanno, I., 2004. Stimulus frequency dependence of the linear relationship between local cerebral blood flow and field potential evoked by activation of rat somatosensory cortex. Neurosci. Res. 48, 147–153.
Vazquez, A.L., Masamoto, K., Kim, S.-G., 2008. Dynamics of oxygen delivery and consumption during evoked neural stimulation using a compartment model and CBF and tissue $PO_2$ measurements. NeuroImage 42, 49–59.
Zheng, Y., Martindale, J., Johnston, D., Jones, M., Berwick, J., Mayhew, J., 2002. A model of the hemodynamic response and oxygen delivery to brain. NeuroImage 16, 617–637.
Zheng, Y., Johnston, D., Berwick, J., Chen, D.M., Billings, S., Mayhew, J., 2005. A three-compartment model of the hemodynamic response and oxygen delivery to brain. NeuroImage 28, 925–939.
Zonta, M., Angulo, M.C., Gobbo, S., Rosengarten, B., Hossmann, K.A., Pozzan, T., Carmignoto, G., 2003. Neuron-to-astrocyte signaling is central to the dynamic control of brain microcirculation. Nat. Neurosci. 6, 43–50.